Journal of the European Ceramic Society **11** (1993) 439–444

Sol–Gel Derived SiO_2–ZrO_2 Nanocomposite Fibers: Influence of Composition, Thermal Treatment and Microstructure on Tensile Strength

Vincenzo M. Sglavo, Roberto Dal Maschio, Gian Domenico Sorarù & Giovanni Carturan

Dipartimento di Ingegneria dei Materiali, via Mesiano 77, I-38050 Trento, Italy

(Received 1 October 1992; accepted 11 November 1992)

Abstract

Fibers of the SiO_2–ZrO_2 system with 70/30 and 50/50 (wt%) compositions were prepared by the sol–gel method, using Si and Zr alkoxides as precursors. Green fibers were heated at different temperatures up to 1500°C. Chemical processes in solution and heating procedures provided a particular microstructure of the final material in which spherical particles of tetragonal zirconia were embedded in an amorphous matrix. The tensile strength of the fibers was determined as a function of cross-sectional area for samples treated at different temperatures with variable heating times. Fractographical analysis allowed determination of fracture toughness. Mechanical properties are discussed in terms of ZrO_2 crystallization (tetragonal habit), fiber densification and microstructure.

Fasern des SiO_2–ZrO_2 Systems mit einem Anteil von 70/30 und 50/50 (Gew.%) wurden über die Sol–Gel Methode hergestellt, wobei Si und Zr Alkoxide als Ausgangsverbindungen dienten. Die rohen Fasern wurden auf verschiedene Temperaturen bis zu 1500°C erhitzt. Chemische Prozesse, die während des Lösens und Erhitzens stattfinden, führen zu einem Mikrogefüge in dem die sphärischen Teilchen des tetragonalen Zirkoniumoxids in eine amorphe Matrix eingebettet sind. Die Zugfestigkeit der Fasern für Proben, die bei verschiedenen Temperaturen und unterschiedlich lang behandelt wurden, wurde als Funktion des Querschnittes betimmt. Eine Analyse der Bruchfläche erlaubte die Bestimmung der Bruchzähigkeit. Die mechanischen Eigenschaften werden in Hinsicht auf die ZrO_2-Kristallisation (tetragonale Kristallform), Faserverdichtung und Mikrogefüge diskutiert.

Des fibres de composition SiO_2–ZrO_2 dans des rapports 70/30 et 50/50 (% en poids) ont été préparées par la methode sol–gel, à partir de précurseurs de type alcoxyde de Si et de Zr. Les fibres crues ont été traitées thermiquement à différentes températures jusqu'à 1500°C. Les procédés chimiques de préparation en solution ainsi que les conditions de traitement thermique permettent l'obtention d'un matériau dont la microstructure particulière consiste en une matrice amorphe dans laquelle sont incluses des particules sphériques de zircone quadratique. La résistance en traction des fibres a été déterminée en fonction de l'aire de la section pour des échantillons soumis à différentes températures et durées de cuisson. L'analyse fractographique permet d'évaluer la ténacité. Les propriétés mécaniques sont discutées en terme de cristallisation de la zircone (phase quadratique), de la densification des fibres et de leur microstructure.

1 Introduction

The SiO_2–ZrO_2 system is quite attractive for the production of glass–ceramic fibers, owing to its valuable chemical and structural properties: the ZrO_2 load may have possible applications for composites in concrete, as substitutes for ZrO_2-containing glass fibers and in high-temperature composites.

In spite of the number of patents and literature claims,[1–7] the mechanical characterization of sol–gel-derived SiO_2–ZrO_2 fibers is still incomplete as regards relationships among preparation procedure, composition, thermal treatment and tensile strength. Thus, while the chemical and rheological restrictions for continuous fiber production have been definitively ascertained, the influence of high-

Journal of the European Ceramic Society 0955-2219/93/$6.00

temperature treatment on densification, microstructure and tensile strength has not yet been established.

In a recent paper[8] some of the authors studied the effects of preparation artifacts and thermal treatments on the tensile strength of $80SiO_2$–$20ZrO_2$ (mol%) fibers.

The aim of this work is the study of the microstructural evolution with heating versus the tensile strength of fibers with zirconia loads of 30 and 50 wt%. Work focuses on the mechanical behavior of samples heated between 900 and 1200°C, at which possible occurrence of tetragonal or monoclinic ZrO_2 and cristobalite may lead to fibers with different microstructures, accounting for changes in mechanical features. More general knowledge of SiO_2–ZrO_2 fibers prepared by the sol–gel technique was gained by the phase characterization of the compositions studied here, carried out in parallel with mechanical tests.

2 Experimental

2.1 Preparation of fibers

The fibers used in this work were prepared by the sol–gel method following the already reported procedure.[7–9] The various steps involved are hydrolysis and condensation of Si–Zr alkoxide solutions, fiber drawing, stabilization and conversion of green fibers to the final product by heat treatment.

Spinning of the viscous solutions, solvent evaporation and other handling procedures have been described elsewhere.[9,10] The nominal compositions of fired products, 30 and 50 wt% of ZrO_2, were calculated from the stoichiometry of the alkoxide precursors. In this report, fibers with $70SiO_2$–$30ZrO_2$ and $50SiO_2$–$50ZrO_2$ (wt%) compositions are indicated as 7S and 5S, respectively.

2.2 Measurements

Green fibers were characterized by differential thermal analysis (DTA), X-ray diffraction (XRD) and density measurements. DTA tests were performed in air on green fibers with a heating rate of 10°C/min up to 1600°C (Fig. 1). XRD analyses, density measurements and TEM (transmission electron microscopy) observations were carried out on samples annealed for 2 h at temperatures in the range 400–1500°C, for general characterization of the two compositions. These analyses were also repeated on the fibers used for mechanical testing. X-Ray spectra were collected on a spectrometer operating at 20 KV with CuK_α radiation and a Ni filter. The Scherrer equation was used to calculate the average diameter of crystals from the width of

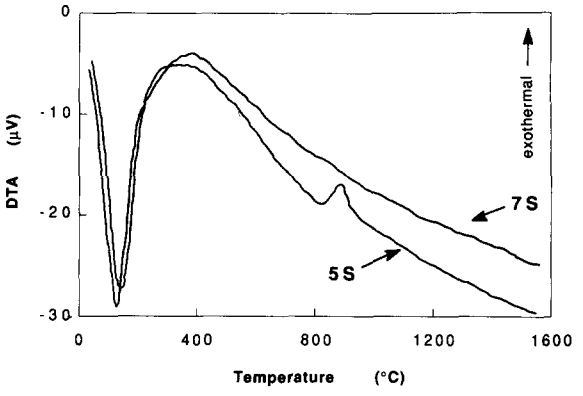

Fig. 1. DTA diagrams for 5S and 7S fibers.

XRD peaks. Evaluation of the apparent density of the fibers previously used for XRD analysis was carried out by means of the Archimedes method, using toluene as fluid.

The tensile strength of single fibers was measured using a universal mechanical testing machine. Testing was conducted according to ASTM D 3379-75 (1982); fibers were mounted with acrylic adhesive on cardboard tabs for aligning and gripping. A 5 mm gage length and a cross-head speed of 2 mm/min were used in all tests.

Due to the non-circular cross-section of the fibers, the fracture load was converted to tensile strength by measuring the cross-sectional area with an optical microscope. Every cross-section was drawn on a paper sheet and the reproduced cross-sections were then weighed to calculate the cross-sectional area.

Tensile tests were performed on fibers heated for 15 min and 10 h at 900 and 1200°C.

3 Results and Discussion

After solvent and by-product release below 400°C, the DTA diagram for 7S fibers does not show evident exothermic effects, while for 5S samples a

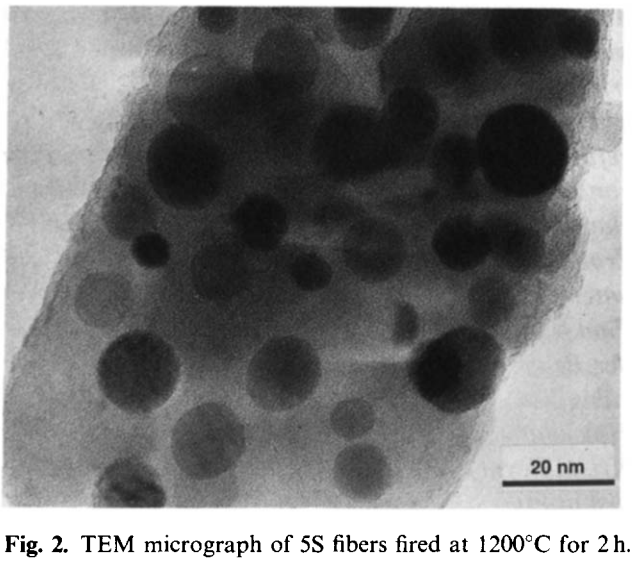

Fig. 2. TEM micrograph of 5S fibers fired at 1200°C for 2 h.

Table 1. Crystalline phases of 7S and 5S fibers fired for 2 h at different temperatures

Temperature (°C)	*7S*	*5S*
800	Amorphous	Amorphous
1 000	t-ZrO_2 (3)	t-ZrO_2 (5)
1 200	t-ZrO_2 (6)	t-ZrO_2 (8)
1 500	t-ZrO_2 (24)	t-ZrO_2 (26)
	Cristobalite (40)	Cristobalite (33)
	Zircon (traces)	Zircon (traces)

Average crystallite diameters in parentheses.

peak emerges at 870°C, which, according to XRD results, can be attributed to crystallization of tetragonal zirconia (Fig. 1).

Phases present in fibers fired at 800, 1000, 1200 and 1500°C for 2 h are reported in Table 1, together with the calculated average diameter of crystallites. XRD analysis indicates that crystallization of tetragonal zirconia (t-ZrO_2) starts between 800 and 1000°C: crystallite dimensions increase from 3–5 nm at 1000°C up to ≈25 nm at 1500°C, apart from zirconia load. At variance with a previous report,[8] the presence of cristobalite is definitely revealed here only for samples heated above 1200°C. TEM observations always revealed spherical crystalline microparticles embedded into an amorphous matrix. A typical TEM micrograph is shown in Fig. 2. Particles size measurement, based on TEM micrographs, agree well with XRD analysis.

The maintenance of ZrO_2 crystals in tetragonal habit without stabilizer is a crucial issue determined by crystal dimensions and the constraining effect of the matrix.[11] The absence of the ZrO_2 tetragonal–monoclinic transformation results from the chemical approach used here,[9,12] which causes high dispersion of Zr oxide in the early stages of the process, so that subsequent crystallization affords tetragonal ZrO_2 with an average crystalline diameter below the critical dimensions.

The evolution of apparent density with temperature is shown in Fig. 3. Theoretical densities for the two different compositions are given for comparison: these were calculated by assuming amorphous silica or α-cristobalite together with t-ZrO_2. The resulting diagram can ideally be divided into two parts. The first, below 1000°C, is characterized by densification of the amorphous matrix, incipient t-ZrO_2 crystallization above 800°C, with a density increase as a function of zirconia content. In the second part, the densification rate is slower, this effect being more pronounced for 5S fibers with the highest amounts of crystallized zirconia.

The experimental evidence may be explained by taking into account the fact that glass matrices in particulate composites show densification behavior which is almost insensitive to inclusions of solids below the percolation threshold (≈16 vol.% for monospheres) defining the lower limit for a contiguous network.[13] In the present case, zirconia contents were 14 and 27 vol.% for 7S and 5S fibers, respectively, so that, as crystalline ZrO_2 separates, densification is affected by the zirconia load, particularly for 5S fibers.

Figures 4 and 5 show tensile strengths for 7S and 5S fibers, respectively. As pointed out by Kamiya *et al.*,[14] a high scattering of strength data, as in the present case, may be caused by several factors, including twisting of fibers and accidental bending or torsion during measurement. With the aim of obtaining a more immediate picture of the relation-

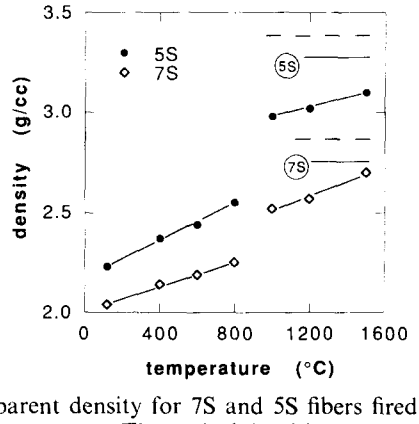

Fig. 3. Apparent density for 7S and 5S fibers fired for 2 h at different temperatures. Theoretical densities are represented by the solid (amorphous silica + t-ZrO_2) and broken (cristobalite + t-ZrO_2) lines.

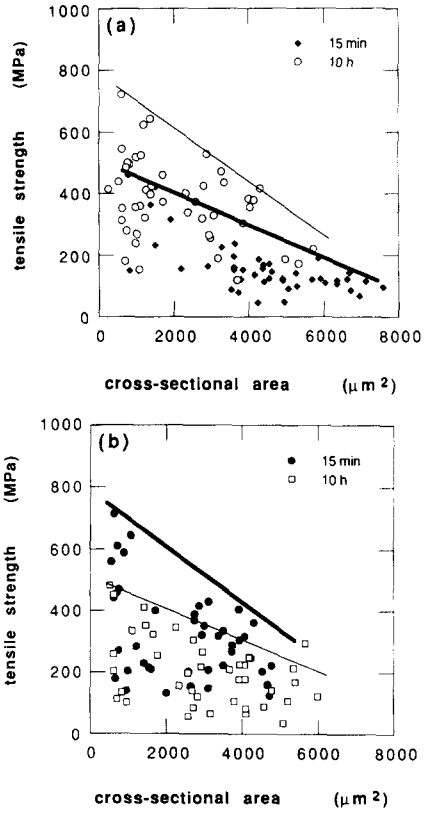

Fig. 4. Tensile strength as function of cross-sectional area of 7S fibers treated at (a) 900°C and (b) 1200°C for different annealing times. The lines represent the envelopes of the strength data.

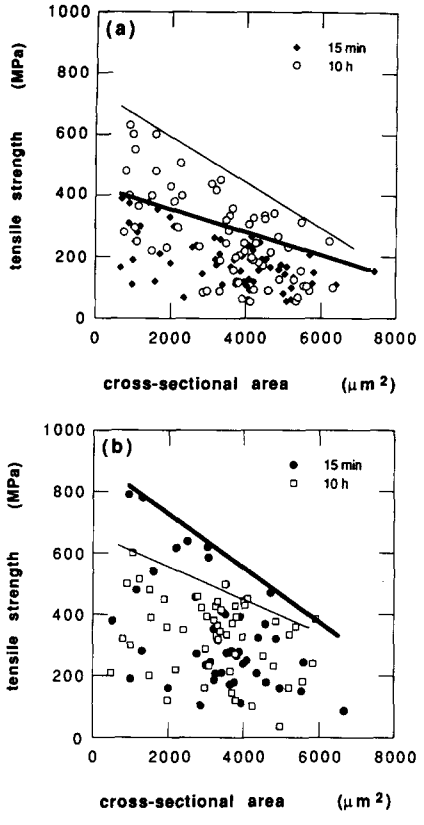

Fig. 5. Tensile strength as function of cross-sectional area of 5S fibers treated at (a) 900°C and (b) 1200°C for different annealing times. The lines represent the envelopes of the strength data.

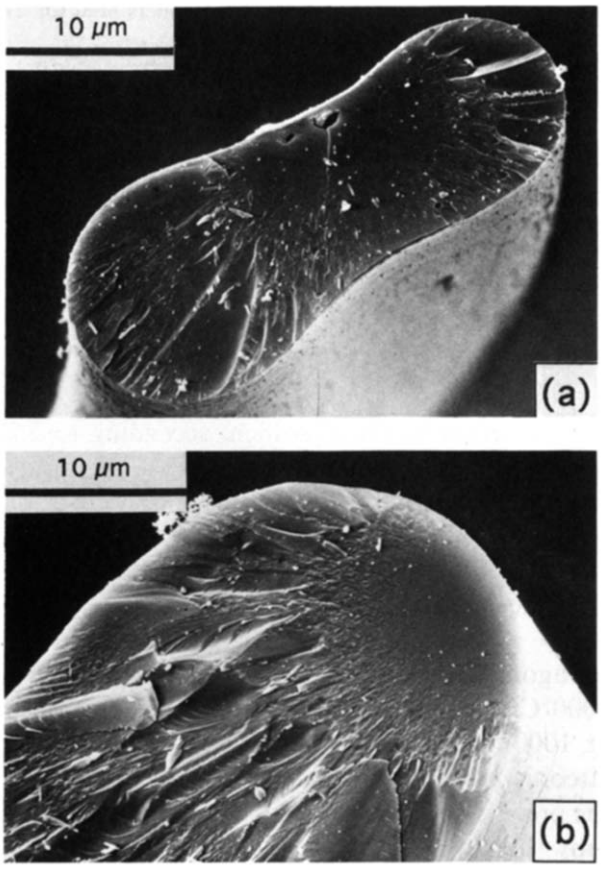

Fig. 6. Fracture morphology of two 7S fibers fired at 1200°C for (a) 10 h and (b) 15 min which had strengths of 220 and 600 MPa, respectively.

ship between tensile strength and cross-sectional area, a line running through the maximum strength values is used to represent the strength of fibers. In all cases, tensile strength depends on cross-sectional area, as expected for brittle fibers, since the probability of finding a critical defect increases with surface and/or volume.

Both compositions at 900°C show a marked strength increase with annealing time (Figs 4(a) and 5(a)). This evidence may be attributed to density increase (Table 2), due to amorphous matrix densification and zirconia crystallization. At 1200°C the tensile strength of 7S fibers annealed for 15 min (Fig. 4(b)) is the same as for fibers annealed at 900°C for 10 h, in spite of the definite density increase occurring at 1200°C; moreover, 10 h annealing at 1200°C causes a decrease in strength (Fig. 4(b)), whereas density remains constant (Table 2).

In contrast, 5S fibers show an increase in strength from fibers heated at 900°C for 10 h to those treated at 1200°C for 15 min. A smaller decrease in strength was observed for fibers treated at 1200°C for 10 h (Fig. 5(b)).

Information on strength-controlling flaws was obtained by accurate examination of fracture surfaces. Defects in all fibers can be divided into three groups: pores, inclusions (Fig. 6(a)) and surface flaws (Fig. 6(b)). Most of the fibers show the classical mirror–mist–hackle fracture morphology for brittle ceramics; also the locus of failure is sometimes evident, particularly for lower strength fibers, in which fracture generally originates from pores or inclusions.

Fracture mirror radius, r, was measured and

Table 2. Density and crystalline phases of 7S and 5S fibers used for mechanical testing

Conditions	*Density (g/cm³)*		*Phases and crystallites dimension (nm)*	
	5S	*7S*	*5S*	*7S*
900°C, 15 min	2·68	2·30	Amorphous	Amorphous
900°C, 10 h	2·74	2·41	t-ZrO_2 (5)	t-ZrO_2 (2)
1200°C, 15 min	3·00	2·55	t-ZrO_2 (6·5)	t-ZrO_2 (5)
1200°C, 10 h	3·05	2·60	t-ZrO_2 (10)	t-ZrO_2 (8)

Average crystallites diameters in parentheses.

Table 3. Mirror constant, A, and fracture toughness, K_{IC}, for 7S and 5S fractured fibers used in mechanical testing

Conditions	A ($MPa\,m^{0.5}$)		K_{IC} ($MPa\,m^{0.5}$)	
	5S	*7S*	*5S*	*7S*
900°C, 15 min	0·83 (0·28)	0·68 (0·49)	0·51 (0·18)	0·39 (0·13)
900°C, 10 h	1·12 (0·43)	1·25 (0·42)	0·81 (0·30)	0·94 (0·40)
1200°C, 15 min	1·31 (0·27)	1·30 (0·47)	0·96 (0·43)	1·01 (0·38)
1200°C, 10 h	1·08 (0·46)	0·92 (0·65)	0·82 (0·35)	0·86 (0·25)

Standard deviation in parentheses.

plotted as function of fracture stress, σ. Points were in agreement with the Mecholsky *et al.*[15] equation:

$$A = \sigma r^{1/2} \quad (1)$$

Results for the mirror constant, A, for 7S and 5S fibers are shown in Table 3.

While the mirror radius is rather easy to measure, critical flaw sizes are much more difficult. However, some of the flaws were measured and the critical stress intensity factor, K_{IC}, was calculated by the well-known equation:[16]

$$K_{IC} = Y\sigma\sqrt{c} \quad (2)$$

where Y is a constant depending on flaw geometry and c the flaw radius. Results are shown in Table 3.

The trends of toughness and mirror constant as a function of thermal treatments parallel the behavior of tensile strength (Figs 4 and 5) for both compositions. This evidence suggests that thermal treatments do not affect the critical flaws population. In fact, as dispersed particles are much smaller than crack sizes, t-ZrO_2 dispersion does not influence critical crack size: the observed variation in strength results entirely from variation in fracture toughness. TEM observations of fibers subjected to different thermal treatments (Fig. 7) do not show any evidence of cracks around or within zirconia particles. This fact agrees with the calculated critical radius of inclusions for crack formation during cooling in particulate composites:[17] for the present systems, the calculated value was about 3 μm, i.e. at least two orders of magnitude greater than the diameter of zirconia particles.

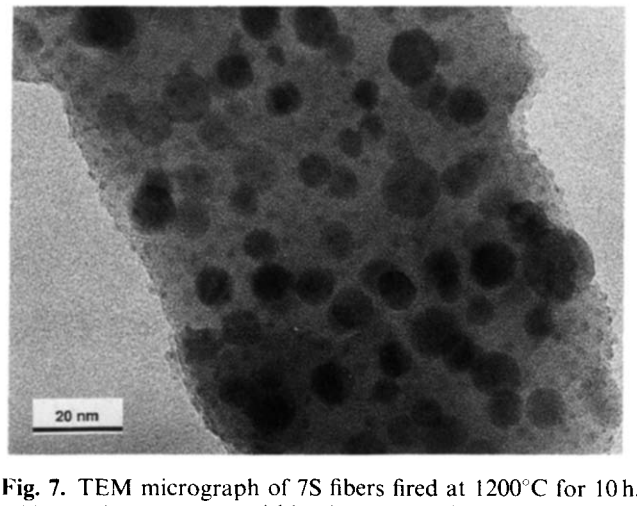

Fig. 7. TEM micrograph of 7S fibers fired at 1200°C for 10 h. No cracks around or within zirconia particles are evident.

Changes in fracture toughness and tensile strength must be correlated to microstructural rearrangements caused by the occurrence of the crystalline phase, as well as by variations in density and chemical composition of the amorphous matrix. The advance of densification and ZrO_2 crystallization, consequent on temperature increase or prolonged annealing times, are responsible for the increase in elastic modulus and fracture energy, in agreement with the observed increase in mechanical resistance. Moreover, it is well known that second-phase dispersion in a brittle material can increase fracture energy by impeding crack propagation.[17–21]

Nevertheless, ZrO_2 crystallization is responsible for the appearance of a residual stress field around and within particles. In particular, the difference in thermal expansion coefficients implies that, on cooling, inclusions are subjected to tensile stress, while the matrix is subjected to radial tensile and tangential compressive stresses.[21] On the other hand, when the external load is applied to the composite, localized stress concentration is generated around and within the particles due to a difference in elastic constants between particle and matrix.

At this point, a detailed relationship between fracture toughness and microstructural features appears a formidable task. The present discussion implies that fracture toughness results from a balance among opposite contributions; this suggests that, up to 1200°C for 15 min, the evolution of microstructure determines an increase of fracture toughness while, for longer annealing times, detrimental contributions start to prevail, leading to the observed strength decrease.

4 Conclusions

SiO_2–ZrO_2 fibers with 70/30 and 50/50 (wt%) compositions were prepared by the sol–gel method.

Final products were composed of spherical particles of tetragonal zirconia embedded in an amorphous matrix.

Fractographic analysis of fractured fibers showed similar trends of toughness and tensile strength as a function of thermal treatments. These results suggest that t-ZrO_2 particles have no effect in altering inherent crack size, strength changes resulting entirely from variations in fracture toughness. The effect of heating on fracture toughness and tensile strength are due to the balance between the increases in density and fracture energy and the parallel increase in tensile residual stress fields and stress concentrations around particles.

References

1. Sakka, S., In *Sol–Gel Technology for Thin Films, Fibers, Preforms, Electronics and Specialty Shapes*, ed. L. C. Klein. Noyes Publications, NJ, 1988, Chapter 7, pp. 140–61.
2. Sowman, H. G., In *Sol–Gel Technology for Thin Films, Fibers, Preforms, Electronics and Specialty Shapes*, ed. L. C. Klein. Noyes Publications, NJ, 1988, Chapter 8, pp. 162–83.
3. Lacourse, W. C., In *Sol–Gel Technology for Thin Films, Fibers, Preforms, Electronics and Specialty Shapes*, ed. L. C. Klein. Noyes Publications, NJ, 1988, Chapter 9, pp. 184–98.
4. Horikiri, S., Tsuji, K., Abe, Y., Fukui, A. & Ichiki, E., US Patent 4,101,615, 18 July 1978; assigned to Sumitomo Chemical Company, Ltd.
5. Borer, A. & Krogseng, G. P., US Patent 3,760,049, 18 September 1973; assigned to Minnesota Mining and Manufacturing Company.
6. Sowman, H. G., US Patent 3,795,524, 5 March 1974; assigned to Minnesota Mining and Manufacturing Company.
7. Brenna, U., Carturan, G., Del Felice, G., Mozzon, M. & Dal Maschio, R., European Patent 0383051-A2, 22 January 1990.
8. Dal Maschio, R., Filipponi, M., Sorarù, Gian D., Carturan, G. & Del Felice, G. M., Tensile strength of SiO_2–ZrO_2 fibers prepared by the sol–gel method: effect of preparation artifacts and thermal treatments. *Am. Ceram. Soc. Bull.*, **71** (1992) 204–12.
9. Brenna, U., Carturan, G. & Sorarù, G. D., Rheological behaviour of solutions affording SiO_2 and SiO_2/ZrO_2 fibers. *J. Non-Cryst. Solids*, **134** (1991) 191–8.
10. Brenna, U., Sglavo, V. M., Sorarù, G. D. & Carturan, G., Viscosity behaviour of SiO_2–ZrO_2 gelling solutions: effect of acetic anhydride addition. *J. Non-Cryst. Solids*, **147 & 148** (1992) 695–8.
11. Nogami, M. & Tomozawa, M., ZrO_2-Transformation-toughened glass–ceramics prepared by the sol–gel process from metal alkoxides. *J. Am. Ceram. Soc.*, **69** (1986) 642–50.
12. Brenna, U., Carturan, G., Ceccato, R. & Mozzon, M., High temperature behavior of ZrO_2–SiO_2 and Al_2O_3–SiO_2 systems obtained by the sol–gel method. In *Proceedings of 4th Ultrastructure Conference*, 1989, J. Wiley & Sons, in press.
13. Brinker, C. J. & Scherer, G. W., *Sol–Gel Science*. Academic Press, NY, 1990, pp. 735–7.
14. Kamiya, K., Takahashi, K., Maeda, T., Nasu, H. & Yoko, T., Sol–gel derived CaO- and CeO_2-stabilized ZrO_2 fibers—conversion process of gel to oxide and tensile strength. *J. Eur. Ceram. Soc.*, **7** (1991) 295–305.
15. Mecholsky, Jun, J. J., Freiman, S. W. & Rice, S. W., Fracture surface analysis of ceramics. *J. Mater. Sci.*, **11** (1976) 1310–19.
16. Evans, A. G., Fracture mechanics determinations. In *Fracture Mechanics of Ceramics*, Vol. 1, ed. R. C. Bradt, D. P. H. Hasselman & F. F. Lange. Plenum Press, NY, 1974, pp. 17–48.
17. Davidge, R. W. & Green, T. J., The strength of two-phase ceramic/glass materials. *J. Mater. Sci.*, **3** (1968) 629–34.
18. Lange, F. F., The interaction of a crack front with a second-phase dispersion. *Phil. Mag.*, **22** (1970) 983–92.
19. Evans, A. G., The strength of brittle composite containing second phase dispersion. *Phil. Mag.*, **26** (1972) 1327–44.
20. Green, D. J. & Nicholson, P. S., Facture of brittle particulate composites. In *Fracture Mechanics of Ceramics*, Vol. 4, ed. R. C. Bradt, D. P. H. Hasselman & F. F. Lange. Plenum Press, NY, 1978, pp. 945–60.
21. Miyata, N. & Jinno, H., Strength and fracture surface energy of phase-separated glasses. *J. Mater. Sci.*, **16** (1981) 2205–17.